Turbulent Entrainment Into Volcanic Plumes: New Constraints From Laboratory Experiments on Buoyant Jets Rising in a Stratified Crossflow

T. J. Aubry, G. Carazzo, A. M. Jellinek

HAL Id: insu-03748836

https://hal-insu.archives-ouvertes.fr/insu-03748836

Submitted on 10 Aug 2022

Turbulent Entrainment Into Volcanic Plumes: New Constraints From Laboratory Experiments on Buoyant Jets Rising in a Stratified Crossflow

T. J. Aubry[1] [ID]**, G. Carazzo[2], and A. M. Jellinek[1]** [ID]

[1]Department of Earth, Ocean, and Atmospheric Sciences, University of British Columbia, Vancouver, British Columbia, Canada, [2]Observatoire Volcanologique et Sismologique de Martinique, Institut de Physique du Globe de Paris, Sorbonne Paris Cité, CNRS, Martinique, France

Abstract Predictions for the heights and downwind trajectories of volcanic plumes using integral models are critical for the assessment of risks and climate impacts of explosive eruptions but are strongly influenced by parameterizations for turbulent entrainment. We compare four popular parameterizations using small scale laboratory experiments spanning the large range of dynamical regimes in which volcanic eruptions occur. We reduce uncertainties on the wind entrainment coefficient β which quantifies the contribution of wind-driven radial velocity shear to entrainment and is a major source of uncertainty for predicting plume height. We show that models better predict plume trajectories if (i) β is constant or increases with the plume buoyancy to momentum flux ratio and (ii) the superposition of the axial and radial velocity shear contributions to the turbulent entrainment is quadratic rather than linear. Our results have important implications for predicting the heights and likelihood of collapse of volcanic columns.

Plain Language Summary One-dimensional models of volcanic plumes can predict whether a volcanic column will collapse and produce devastating pyroclastic flows or rise as a buoyant plume. In this case, 1-D models can predict the height at which the volcanic plume will inject gases and ash, which is critical to make predictions for the climate impact of an eruption, as well as to assess ash fallout hazard. In these models, the mixing between the plume and the ambient atmosphere is parameterized. Uncertainties on this parameterization are very large and undermine all model predictions, such as the height a volcanic plume. In this study, we use small-scale laboratory experiments to improve constraints on the most used parameterizations for mixing between a volcanic plume and the atmosphere. The experimental data set used spans the large range of dynamical regimes in which explosive volcanic eruptions occur. Our result significantly reduce uncertainties for predicting (i) under which conditions an eruptive column will collapse and produce pyroclastic flows and (ii) what eruption magnitude is required for a volcanic plume to reach the stratosphere (the higher part of the atmosphere) and significantly reduce Earth's surface temperature.

1. Introduction

A major control on explosive volcanic plume behavior is the turbulent entrainment of ambient atmosphere into the plume. This process is parameterized in one-dimensional integral models of volcanic plumes. Important parameters, such as the wind entrainment coefficient, are subject to uncertainties of up to an order of magnitude (e.g., Hewett et al., 1971; Suzuki and Koyaguchi, 2015), and values used in the latest volcanic plume model intercomparison study vary by a factor of 2 among modeling groups (Costa et al., 2016). Plume height predictions are consequently subject to uncertainties of up to a factor 3 (Figure 1, left), with critical implications for how to evaluate the climate impacts of explosive eruption (e.g., Robock, 2000). Uncertainties on entrainment parameters also affect the predictions for the collapse of volcanic plumes and the production of devastating pyroclastic flows (Degruyter & Bonadonna, 2013; Jessop et al., 2016).

In the classical entrainment parameterization developed for a buoyant jet rising into a quiescent environment, the radial entrainment velocity u_ϵ is proportional to the upflow velocity u:

$$u_\epsilon = \alpha |u| \ , \tag{1}$$
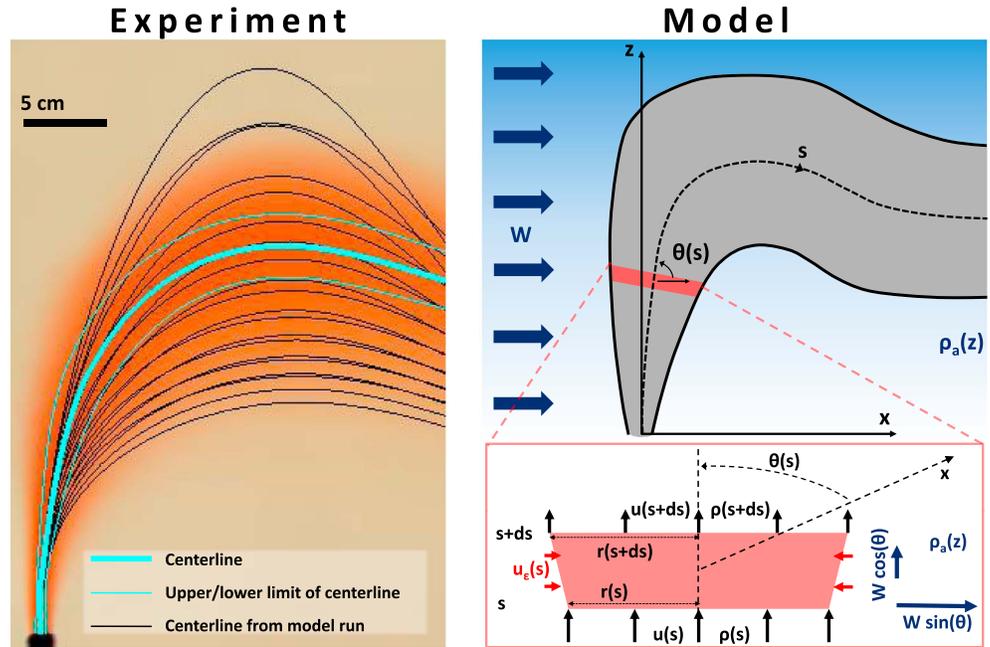
Experiment

Model

Figure 1. (left) Buoyant jet, observed centerline (cyan lines), and model centerlines (black lines) for one experiment from the Carazzo et al. (2014) data set. The picture shows the average of $\geqslant 300$ frames taken during the experiment. The thick and thin cyan lines show the plume centerline and the 95% confidence envelope of the centerline as found by a semi-automatic script. Black lines show model trajectories for model 2 for one sample of source and environmental conditions (i.e., one Monte Carlo simulation, cf. section 3), for all tested values of β and $m = 1$ or $m = 2$. (right) Cartoon of a rising plume (top) and of the control volume (bottom) used to derive conservation equations (4)–(8). Modified from Aubry et al. (2017).

where α is the radial entrainment coefficient. To extend this parameterization to an environment with a horizontal crossflow (e.g., wind), Hoult et al. (1969) propose that the axial and radial velocity differences between the jet and the ambient fluid contribute linearly to the entrainment rate, such that

$$u_\epsilon = \alpha|u - w\cos(\theta)| + \beta|w\sin(\theta)| \ . \tag{2}$$

Here θ is the local inclination of the plume with respect to the horizontal (Figure 1, right), w the local speed of the crossflow, and β is the wind entrainment coefficient. Devenish et al. (2010) build on Hoult et al. (1969) and propose a less restrictive power law parameterization of the following form:

$$u_\epsilon = ((\alpha|u - w\cos(\theta)|)^m + |\beta w\sin(\theta)|^m)^{\frac{1}{m}} \ . \tag{3}$$

In this treatment, $m \geqslant 1$ is a constant. As m increases, the contribution to u_ϵ of the largest term among $\alpha|u - w\cos(\theta)|$ and $|\beta w\sin(\theta)|$ increases. In terms of predictions for plume height, Devenish et al. (2010) find a better agreement with large eddy simulations for $m = 1.5$.

Although equation (3) is the most general entrainment parameterization, the values for m, α, and β vary widely in the literature. This variability is a major cause of uncertainty in integral models of volcanic plumes (Costa et al., 2016). In the majority of models, with the exception of Devenish et al. (2010), the exponent m is taken to be 1. The radial entrainment coefficient α is either imposed constant with values varying between 0.05 and 0.17 (Chen & Rodi, 1980; Morton et al., 1956), or variable with the distance from the source due to local buoyancy effects (Fischer et al., 1979; Kaminski et al., 2005). The wind entrainment coefficient β is commonly taken constant with values varying between 0.1 and 1 (Bursik, 2001; Hewett et al., 1971; Suzuki & Koyaguchi, 2015), but it can also vary with the distance from the source (Folch et al., 2016). Other parameterizations include a variable coefficient α but a constant ratio β/α (Aubry et al., 2017). These large uncertainties in the values of the parameters used in equation (3) lead to important differences in the predictions of jet maximum height and trajectory (Figure 1, left).

The major aim of this study is to evaluate, calibrate, and compare the different entrainment coefficient models available in the literature (section 2) to reduce uncertainties in modeling of volcanic plumes, and more generally buoyant jets. To this end, we use an experimental data set spanning the full range of dynamical conditions in which explosive volcanic eruptions occur, and Monte Carlo simulations to account for experimental uncertainties (section 3). In section 4, we show the constraints obtained on the parameters (m, α, β, or $\frac{\beta}{\alpha}$) used in the tested models and demonstrate that important differences exist among the performance of these models. We briefly discuss our results in section 5 and summarize our main conclusions in section 6.

2. Model

Following Morton et al. (1956) and Hoult et al. (1969), we use a plume-centered system, where s denotes the curvilinear abscissa along the plume centerline. For "Top-Hat" radial dependence of the plume properties, the conservation equations of mass, axial and radial momentum, and buoyancy fluxes for the control volume in Figure 1 (right) are

$$\frac{dx}{ds} = \cos(\theta) \qquad , \qquad \frac{dz}{ds} = \sin(\theta),$$ (4)

$$\frac{d}{ds}\left(\rho u r^2\right) = 2\rho_a r u_\epsilon,$$ (5)

$$\frac{d}{ds}\left(\rho u^2 r^2\right) = \left(\rho_a - \rho\right) g r^2 \sin(\theta) + w \cos(\theta)\frac{d}{ds}\left(\rho u r^2\right),$$ (6)

$$\left(\rho u^2 r^2\right)\frac{d\theta}{ds} = \left(\rho_a - \rho\right) g r^2 \cos(\theta) - w \sin(\theta)\frac{d}{ds}\left(\rho u r^2\right),$$ (7)

$$\frac{d}{ds}\left(g' u r^2\right) = -N^2 u r^2 \sin(\theta),$$ (8)

where x and z are the horizontal and vertical distance from the source, r is the jet radius (orthogonal to s), g is the Earth's gravity acceleration, ρ is the jet density, ρ_a is the density of the atmosphere, $g' = g\left(\rho_a - \rho\right)/\rho_a$ is the jet reduced gravity, and N is the atmospheric Brunt-Väisälä frequency. The turbulent entrainment rate u_ϵ is parameterized by using equation (3) together with four entrainment closures commonly used in the literature:

1. Model 1 (Hewett et al., 1971) uses constant values for α and β. We perform the calculations for $\alpha = 0.05 - 0.17$ with increments of 0.01, and $\beta = 0.1 - 1$ with increments of 0.1, consistent with values found in the literature.
2. Model 2 (Girault et al., 2016; Kaminski et al., 2005) uses a constant value for β and a variable coefficient α:

$$\alpha = 0.0675 + \left(1 - \frac{1}{A}\right)\mathcal{R}i + \frac{r}{2}\frac{d\ln(A)}{dz},$$ (9)

where A is a dimensionless shape function that depends on the flow structure (see, e.g., Carazzo et al., 2006, 2008), z is the vertical distance from the source, and $\mathcal{R}i = rg'/u^2$ is the local Richardson number.
3. Model 3 (Folch et al., 2016) uses variable coefficients α and β. This model combines the parameterization proposed by Kaminski et al. (2005) for the radial entrainment coefficient α (equation (9) and the parameterization proposed by Tate (2002) for the wind entrainment coefficient β based on laboratory experiments from previous studies:

$$\beta = 0.34 \left(\sqrt{2|\mathcal{R}i|}\,\mathcal{W}^*\right)^{-0.125}.$$ (10)

Here $\mathcal{W}^* = w/u_0$ and the subscript $_0$ denotes a value at the source.
4. Model 4 (Aubry et al., 2017) uses a variable coefficient α and a constant ratio β/α at any distance from the source. This model combines the parameterization proposed by Kaminski et al. (2005) for the radial entrainment coefficient α (equation (9) and keeps β/α constant because it enables good predictions of plume height by a scaling law through a large range of $\mathcal{R}i$, where α is expected to vary. However, the scaling on which their results are based uses several simplifying assumptions and the proposed parameterization has not been tested in an integral model for buoyant jets. We perform the calculations for $\beta/\alpha = 4 - 12$ with increments of 1.

In the four models, we performed calculations for $m = 1 - 2$ with increments of 0.25.

3. Data and Methods

The trajectory (x, z) predicted by equations (3)–(8) together with the four models for entrainment coefficient will be compared to measured trajectories (maximum tracer intensity) of laboratory buoyant jets rising in a density-stratified crossflow. These experiments are presented in detail in Carazzo et al. (2014). The full experimental data set spans almost the entire range of Ri_0 and W_0^* in which explosive eruptions occur and cover a much larger parameter space than previous studies (Carazzo et al., 2014).

The source and environment parameters as well as the associated uncertainties were carefully measured for the 27 experiments and are reported in Aubry et al. (2017). We obtained the centerline of the jet and the associated uncertainty for each experiment from the stack of all images recorded with digital video camera using a semi-automatized script looking for maximum tracer intensity. The duration of an experiment is much longer than the plume rise timescale, so that transient turbulent features (e.g., eddies) are removed when stacking all images together. Figure 1 (left) shows an example of experimental buoyant jet and obtained centerline trajectory.

To test how well a given model with specified entrainment parameters values reproduce the plume trajectory of an experiment, we first calculate the standardized root-mean-square error on the plume trajectory for experiment i as

$$e_i = \left(\frac{\int_0^{x^{\max}} \left(z_{\mathrm{mod}} - z_{\mathrm{obs}} \right)^2 dx}{\int_0^{x_{\mathrm{obs}}^{\max}} z_{\mathrm{obs}}^2 dx} \right)^{1/2}, \tag{11}$$

where z_{mod} is the modeled height of the centerline, z_{obs} the observed height, $x_{\mathrm{obs}}^{\max}$ is the horizontal distance from the source where the maximum plume height is reached for the observed centerline, and $x^{\max}$ is the largest value between $x_{\mathrm{obs}}^{\max}$ and $x_{\mathrm{mod}}^{\max}$ (same as $x_{\mathrm{obs}}^{\max}$ but for the model trajectory).

Next, we find the total weighted root-mean-square error of a model prediction for plume trajectories with specified entrainment parameter values as

$$E = \left(\frac{1}{n} \sum_{i=1}^{n} \frac{e_i^2}{\left(\Delta e_i \right)^2} \right)^{1/2}, \tag{12}$$

where $n = 27$ is the number of experiments and the weights Δe_i are the 95% observational uncertainty on e_i (cf. supporting information S1 for the detailed calculation of Δe_i). These weights give more importance to experiments with smaller observational error. The error E is then calculated for each entrainment model (1–4) and each possible combination of entrainment parameters value (α, β, m, and/or β/α). Note that E is nondimensional and expressed as a fraction of the observational uncertainty. For example, if a model has an error of 1.3, it means that the model error is 30% larger than the error on plume trajectory attributable to experimental uncertainties alone.

Last, to account for experimental uncertainties, we use a Monte Carlo method to generate 100 sets of experimental parameters. For each experiment and each parameter (e.g., exit velocity or plume trajectory), we assume a Gaussian distribution centered on the measured value with standard deviation chosen to match the estimated 95% confidence interval. These distribution parameters are provided in Table S1 for source (e.g., exit velocity U_0) and environment (e.g., wind speed w) parameters for all experiments. We then draw 100 samples of each variable and run the four models across all combination of entrainment parameters to obtain 100 values of the error E for each entrainment model and set of entrainment parameter values. For a given model, we consequently find the best (i.e., by minimizing error E) set of entrainment parameters for each of the 100 Monte Carlo simulations and obtain the probability distributions of the entrainment parameters of each model. In addition, the distribution of pairwise differences in error between two models quantifies the probability for a model to outperform another.

4. Results

4.1. Best Set of Entrainment Parameters for Each Model

For each entrainment model (columns) and each parameter (rows), Figure 2 shows (i) the frequency at which a value of the parameter minimizes the error E across all Monte Carlo simulations (red histograms) and (ii) the minimum error E obtained for each tested value of the parameter (black dots). Thus, red histograms show
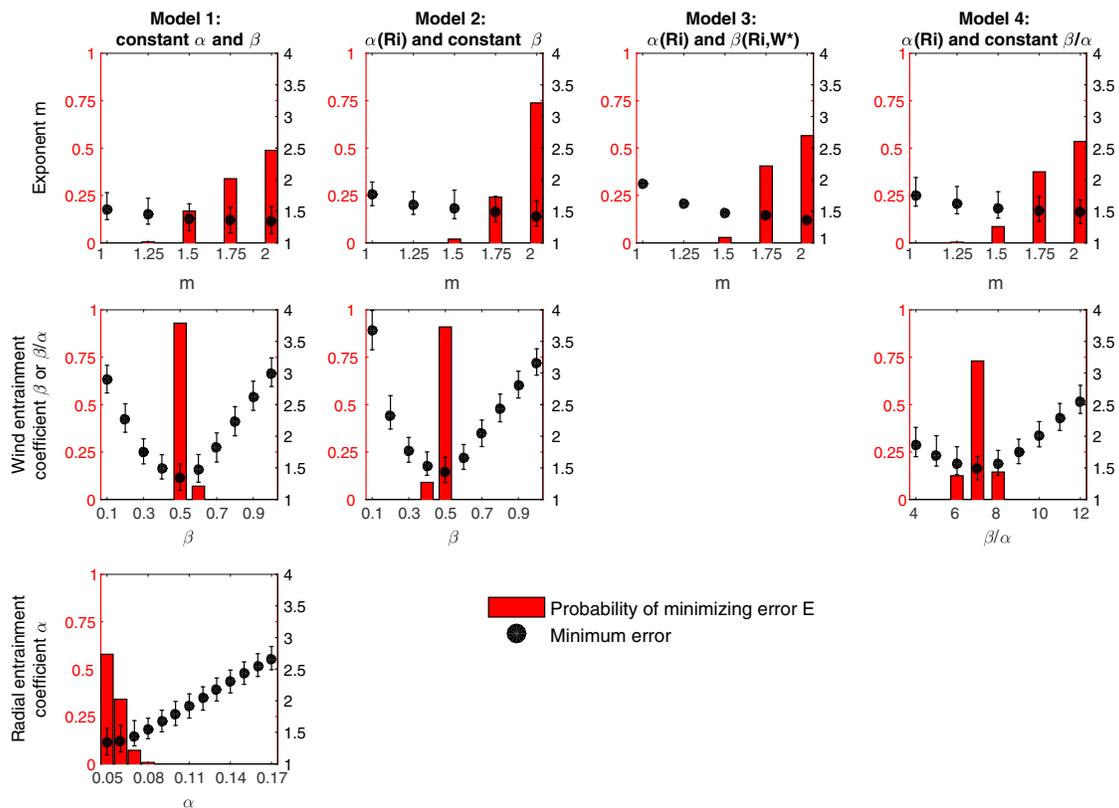
Figure 2. Values of plume model parameters minimizing the error on centerline trajectory (equation (12). Each column of plots shows results related to one entrainment model, while each row of plots shows results related to one type of model parameter. On each plot, red bars (left red axis) show the distribution (across all Monte Carlo simulations) of the parameter values for which the error E on centerline trajectory is minimized. Black dots (right black axis) show the minimum error on centerline trajectory for a fixed value of the model parameter considered. Dots show the mean error and error bars are the 95% confidence interval.

the likelihood that a given parameter value minimizes the error E and black dots show the sensitivity of E to the value of the same parameter, for each model.

The first row of plots in Figure 2 shows results for the exponent m in equation (3). For models 1 and 4, and models 2 and 3, the error on trajectory E is minimized in more than 95% of the Monte Carlo simulations when $m \geqslant 1.5$ and $m \geqslant 1.75$, respectively (as shown by red histograms). The error is sensitive to the value of m: E varies by as much as 0.5 (i.e., 50% of experimental uncertainty on plume trajectories) for the tested values of m.

In the second row of Figure 2, we show results for the wind entrainment parameter β for models 1 and 2, and the ratio $\frac{\beta}{\alpha}$ for model 4. Model 3 parameterize β using equation (10) and its value is thus not specified. The error E is systematically minimized for $\beta = 0.5$–0.6 with model 1 and for $\beta = 0.4$–0.5 with model 2, with $\beta = 0.5$ being the best value in more than 90% of the Monte Carlo simulations for both models. For model 4, the values $\frac{\beta}{\alpha} = 6$–8 minimize E. Models 1 and 2 are very sensitive to β with the minimum error E varying between 1.2 and 4 depending on the value of β. Model 4 is less sensitive to the value of $\frac{\beta}{\alpha}$ with the error E varying between 1.5 and 2.5.

In the third row of Figure 2, we show results for the radial entrainment parameter α for model 1. Models 2–4 use equation (9) for α, and its value is thus not specified. The values $\alpha = 0.05$–0.07 minimize E for model 1, with E ranging from $\simeq 1.4$ for $\alpha = 0.05$ to $\simeq 2.5$ for $\alpha = 0.17$.

4.2. Best Model for Entrainment Coefficients

Figure 3 shows the distribution of pairwise error differences for the six possible pairs of models. These distributions account for both observational uncertainties, and uncertainties on entrainment parameters constrained from Figure 2 (cf. Figure 3's caption).
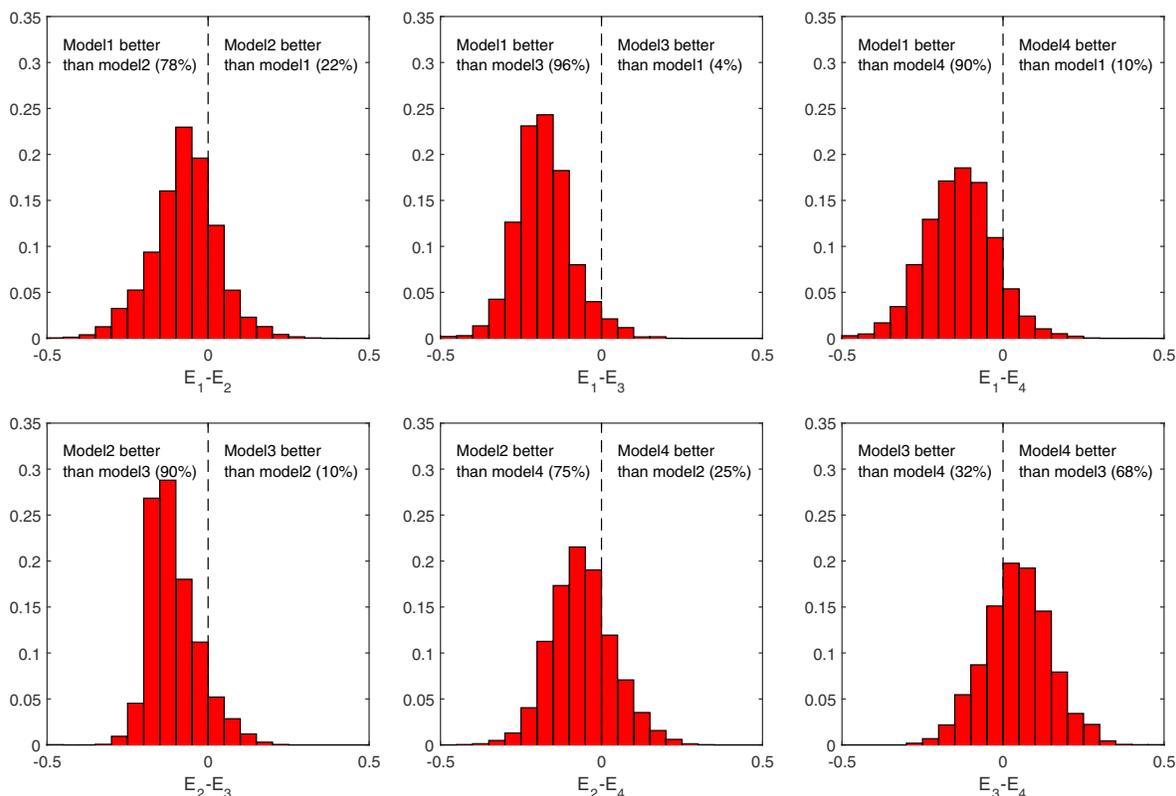
Figure 3. Distribution of pairwise differences of error on centerline trajectory E, for each pair of model. For a given model i, we sampled 1,000 sets of parameters from the distributions shown in Figure 2. We thus obtain 100,000 values of E_i, the error for model i, across all Monte Carlo simulations. The resulting distribution of pairwise differences is shown in this figure and account for both observational and model parameter uncertainty. For two models i and j, $E_i - E_j$ is positive if model j predicts centerline trajectories better than model i, and vice versa. The estimated probability for a model to outperform the other one is annotated on each plot.

The only difference significant at the 95% level is between models 1 and 3, with model 1 having a smaller error in 96% of the samples. However, Figure 3 shows some clear trends in model performance. Model 1 performs better than other models (with a confidence level of 78 to 96%), while model 2 outperforms models 3 and 4 (with a confidence level of 75 to 90%) and model 4 outperforms model 3 in 68% of the samples. The magnitude of pairwise error differences also shows that the error is moderately sensitive to the choice of entrainment models, compared to the choice of entrainment parameter values for each model. Indeed, most error differences do not exceed 0.3 (30% of the observational uncertainties) with highest differences of ≃0.5. In contrast, the choice of β in models 1 or 2 was resulting in error differences of up to 2.5, for example.

5. Discussion

5.1. New Constraints on Entrainment Parameters and Implications for Volcanic Plume Modeling

The constraints obtained on entrainment parameters (m, α, and β) in Figure 2 show notable differences with the values most commonly used in models of volcanic plume. First, most modelers use a value of $m = 1$ (e.g., Degruyter and Bonadonna, 2012; Mastin, 2014; Woodhouse et al., 2013), except the Devenish model which uses $m = 1.5$ (Devenish, 2016; Devenish et al., 2010). Our results are more consistent with Devenish et al. (2010) and show that values of m between 1.5 and 2 decrease the error on plume trajectories by up to 0.5.

Second, Figure 2 suggests that $\beta = 0.4–0.6$ minimize errors in plume trajectories, for both models 1 and 2. Although several models of volcanic plume use $\beta = 0.5$, the range commonly used is 0.5–0.9 (Costa et al., 2016). Our results show that higher values in this range may result in large error on plume trajectories. The compatibility of our results for β with previous studies using a value of $m = 1$ suggests that the value of β is only weakly sensitive to the value of m.
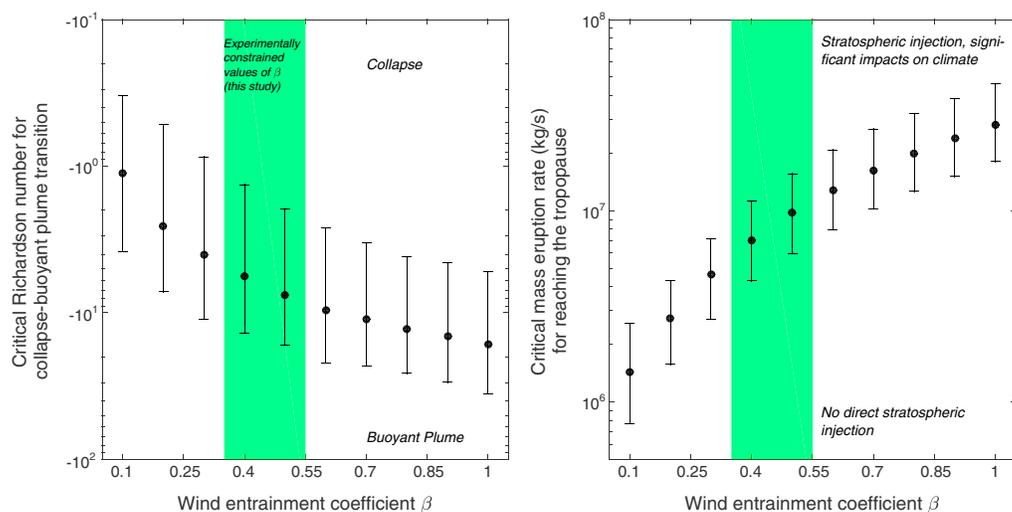
Figure 4. (left) Critical Richardson number at which the transition from buoyant plume to collapsing plume occurs as a function of the wind entrainment coefficient β. (right) Critical mass eruption rate required to cross the tropopause as a function of β. For both plots, we used the model of volcanic plume of Degruyter and Bonadonna (2012) with entrainment coefficients parameterized as in Model 2, $m = 2$, and ignored the effects of condensation of water vapor. Atmospheric conditions correspond to those during the second phase of the 2011 Cordón Caulle eruption, which occurred under strong winds, and were retrieved from the National Centers for Environmental Prediction-National Center for Atmospheric Research reanalysis (Kalnay et al., 1996). Calculations were performed for a range of values of β corresponding to values previously published, and the green shading highlight the values for model 2 constrained in this study. Dots and error bars show the mean and 95% confidence intervals obtained with 300 Monte Carlo simulations where we randomly sampled the source temperature (800–1500 K) and gas content (0.01–0.07 wt %). For Figure 4 (left) (critical Richardson number), the vent radius was also randomly sampled (10–100 m), while for Figure 4 (right) (critical mass eruption rate), the source Richardson number was randomly sampled (-10^{-4}–10^{-2}).

Third, for model 3, the range of 6–8 found for $\frac{\beta}{\alpha}$ in Figure 2 is in remarkable agreement with the results of Aubry et al. (2016), even though this previous study used an analytical scaling (relating plume height to source conditions and environmental parameters) and plume height measurement to constrain this ratio.

Last, for model 1, we find values of α corresponding to values usually found for momentum-driven jets, consistent with $|Ri_0| \leqslant 10^{-1}$. These optimal values of α are for a plume rising under a crossflow, and with $m = 1.5$–2 in equation (3). Previous studies mostly constrained α using $m = 1$, and in the absence of crossflow.

These improved constraints on entrainment parameterizations have important implications for the modeling of volcanic plumes. For example, the main source of uncertainty on volcanic plume height, which governs the lifetime of ash and aerosols in the atmosphere, is the wind entrainment coefficient β (e.g., Woodhouse et al., 2015). In particular, Figure 4 (right) shows that the minimum mass eruption rate required for a volcanic plume to reach the tropopause is uncertain by more than 1 order of magnitude for values of β ranging from 0.1 to 1. The new constraints found in this study result in an uncertainty of a factor of 2. The stability of volcanic plumes, which controls the production of pyroclastic flows, is also determined by the values of entrainment coefficients (Degruyter & Bonadonna, 2013). Figure 4 (left) shows that the critical Richardson number at the vent above which an eruptive column collapses is subject to uncertainties of 1 order of magnitude as a consequence of uncertainties on β. This uncertainty is again significantly reduced thanks to the constraints on β provided in this study.

5.2. Parameterization of Entrainment Coefficients and Future Work

Although our study gives some insights into which models of entrainment parameters best reproduce experimental trajectories, only one pairwise comparison exhibits differences significant at the 95% confidence level (three pairs at the 90% level). In general, it appears that model 3, which assumes that β decreases with Ri, has larger errors than models that assume a constant β (models 1 and 2) or β increasing with Ri.

To understand how entrainment coefficients α and β depend on regime parameters Ri and $\mathcal{W}^*$, we assess which values of α and β minimize the error e (equation (11) for individual experiments. We then assume relationships of the form $\alpha = C_1(Ri_0)^{r_1}(\mathcal{W}_0^*)^{w_1}$ and $\beta = C_2(Ri_0)^{r_2}(\mathcal{W}_0^*)^{w_2}$ and use multilinear regression to find
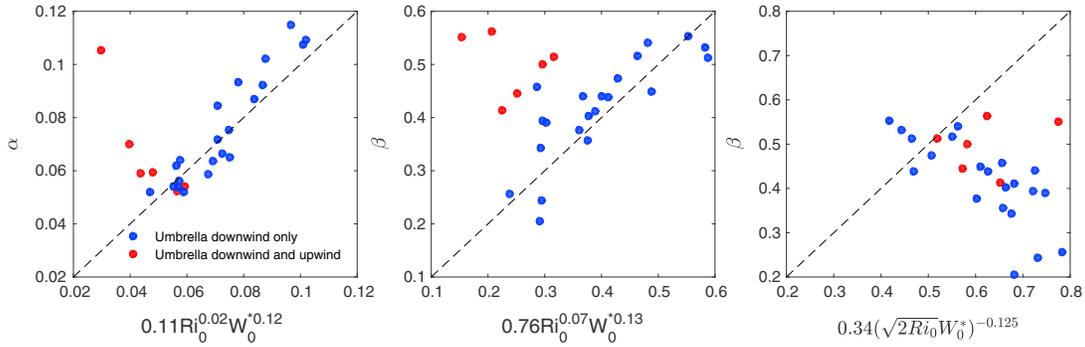
Figure 5. Estimated value of α or β compared to functions of the form $C_1 Ri_0^{r_1} W_0^{*w_1}$. (left and middle) Fit parameters C_1, r_1, and w_1 are estimated using a multilinear regression between α or β, and Ri_0 and W_0^{*w}, on a log scale. Only plumes for which the umbrella spreads only downwind (blue) are used to perform multilinear regressions. (right) The estimated values of β as a function of the paramaterization used in model 3. Dashed lines show the 1:1 ratio. The estimates of α and β are subject to large uncertainties which are not shown for clarity.

the values of fitting coefficients (C_1, C_2, r_1, r_2, w_1, and w_2) minimizing the least squares error, on a log scale. The chosen form for these relationships has no physical basis although it is similar to parameterizations used in other models (e.g., β for model 3, Folch et al., 2016). However, the signs of the exponent provide a simple test on whether entrainment coefficients decrease or increase with the regime parameters $\mathcal{W}_0^*$ and Ri_0.

Figure 5 (left and middle) shows the estimated values of α and β as a function of values predicted by the regression against $\mathcal{W}_0^*$ and Ri_0. We perform regressions using only data from plumes for which the umbrella spreads only downwind, because the dependence of entrainment coefficients on both Ri_0 and $\mathcal{W}_0^*$ in this regime is evident. We find the best fit relationships

$$\alpha = 0.11 Ri_0^{0.02} \mathcal{W}_0^{*0.12} \tag{13}$$

$$\beta = 0.76 Ri_0^{0.07} \mathcal{W}_0^{*0.13} . \tag{14}$$

Figure 5 thus suggests that both α and β increase with $\mathcal{W}_0^*$ and Ri_0 although the dependence on these two parameters is weak. In addition, when constraining values of α and β for individual experiments, uncertainties on source and environmental parameters as well as the plume trajectory result in very large uncertainties. Consequently, there is only a $\geqslant$90% confidence level that coefficients w_1, w_2, and r_2 in the regression are positive (75% for r_1).

Figure 5 (right) shows the estimated values of β as a function of the parameterization of model 3 (Folch et al., 2016; Tate, 2002) and source values $\mathcal{W}^*$. The predicted values and the estimates are anticorrelated at the 95% confidence level despite experimental uncertainties.

Overall, Figure 5 explains the results of Figure 3. Model 3 is outperformed by other models because α and β seem to slightly increase, not decrease, with increasing values of $\mathcal{W}_0^*$ and Ri_0. The lack of significance of these trends causes differences between models 1, 2, and 4 to be not significant at the 95% level. The most significant trend is the increase of α and β with $\mathcal{W}_0^*$ for plumes spreading downwind only and it can be interpreted using the results of Aubry et al. (2017). They find that as crossflow speed increases, tracer profiles in the plume do not remain similar downwind, becoming skewed to the downwind side of the plume which suggests a larger downwind entrainment. This increased downwind entrainment may explain why the model better fits trajectories with larger values of α and β as $\mathcal{W}_0^*$ increases. However, the trends from Figure 5 remain challenging to quantitatively interpret because of their low ($\leqslant$90%) significance caused by uncertainties on individual values of α and β. In addition, local plume properties (velocity and density) were not measured in the Carazzo et al. (2014) experiments so that we can only infer how mean entrainment coefficients depend on source and environmental regime parameters, while parameterizations of models 2, 3, and 4 express relationships between local entrainment rates and local regime parameters. Laboratory experiments covering a large range of parameter space with measurements of local plume properties would thus help improve our understanding of the impact of crossflows on turbulent entrainment in buoyant jets.

6. Conclusions

In this study, we constrain and compare four popular parameterizations of entrainment coefficients involved in equation (3) using small-scale laboratory experiments. We demonstrate that values of the wind entrainment coefficient β between 0.4 and 0.6 and that values of m between 1.5 and 2 minimize error on downwind plume trajectories for these experiments. The latter constraint implies that a quadratic superposition of the axial and radial velocity gradient contributions is better than a linear superposition. In addition, we show that models where β is constant or increases with the plume Richardson number are better than the tested model where β decreases with the Richardson number. Our results also suggest that entrainment coefficients depend on the ratio of the wind velocity to the ascent velocity of the plume, although experiments with local measurement of the plume properties will be required to confirm the trends we exhibit (e.g., 3-D measurements of the average velocity and density, or at least 2-D measurement in the plan defined by the exit velocity and the wind field). Our improved constraints on entrainment parameterizations in volcanic plume models have implications for key predictions for explosive eruptions. These include the height and stability of volcanic columns and the likelihood for the production of pyroclastic flows, as well as the magnitude required for an explosive eruption to reach the stratosphere and have a long-lasting impact on climate.

References

Aubry, T. J., Jellinek, A. M., Carazzo, G., Gallo, R., Hatcher, K., & Dunning, J. (2017). A new analytical scaling for turbulent wind-bent plumes: Comparison of scaling laws with analog experiments and a new database of eruptive conditions for predicting the height of volcanic plumes. *Journal of Volcanology and Geothermal Research*, *343*, 233–251. https://doi.org/10.1016/j.jvolgeores.2017.07.006

Aubry, T. J., Jellinek, A. M., Degruyter, W., Bonadonna, C., Clyne, V. R. M., & Quainoo, A. (2016). Impact of global warming on the rise of volcanic plumes and implications for future volcanic aerosol forcing. *Journal of Geophysical Research: Atmospheres*, *121*, 13,326–13,351. https://doi.org/10.1002/2016JD025405

Bursik, M. (2001). Effect of wind on the rise height of volcanic plumes. *Geophysical Research Letters*, *28*, 3821–3824. https://doi.org/10.1029/2001GL013393

Carazzo, G., Girault, F., Aubry, T. J., Bouquerel, H., & Kaminski, E. (2014). Laboratory experiments of forced plumes in a density-stratified crossflow and implications for volcanic plumes. *Geophysical Research Letters*, *41*, 8759–8766. https://doi.org/10.1002/2014GL061887

Carazzo, G., Kaminski, E., & Tait, S. (2006). The route to self-similarity in turbulent jets and plumes. *Journal of Fluid Mechanics*, *547*, 137–148. https://doi.org/10.1017/S002211200500683X

Carazzo, G., Kaminski, E., & Tait, S. (2008). On the dynamics of volcanic columns: A comparison of field data with a new model of negatively buoyant jets. *Journal of Volcanology and Geothermal Research*, *178*(1), 94–103. https://doi.org/10.1016/j.jvolgeores.2008.01.002

Chen, C. J., & Rodi, W. (1980). Vertical turbulent buoyant jets: A review of experimental data. *NASA STI/Recon Technical Report A*, *80*, 23,073.

Costa, A., Suzuki, Y., Cerminara, M., Devenish, B., Ongaro, T. E., Herzog, M., … Bonadonna, C. (2016). Results of the eruptive column model inter-comparison study. *Journal of Volcanology and Geothermal Research*, *326*, 2–25. https://doi.org/10.1016/j.jvolgeores.2016.01.017

Degruyter, W., & Bonadonna, C. (2012). Improving on mass flow rate estimates of volcanic eruptions. *Geophysical Research Letters*, *39*, L16308. https://doi.org/10.1029/2012GL052566

Degruyter, W., & Bonadonna, C. (2013). Impact of wind on the condition for column collapse of volcanic plumes. *Earth and Planetary Science Letters*, *377*, 218–226. https://doi.org/10.1016/j.epsl.2013.06.041

Devenish, B. (2016). Estimating the total mass emitted by the eruption of Eyjafjallajökull in 2010 using plume-rise models. *Journal of Volcanology and Geothermal Research*, *326*, 114–119. https://doi.org/10.1016/j.jvolgeores.2016.01.005

Devenish, B., Rooney, G., Webster, H., & Thomson, D. (2010). The entrainment rate for buoyant plumes in a crossflow. *Boundary-Layer Meteorology*, *134*, 411–439. https://doi.org/10.1007/s10546-009-9464-5

Fischer, H., List, E., Koh, R., Imberger, J., & Brooks, N. (1979). *Mixing in inland and coastal waters* (pp. 315–389). New York: Academic Press.

Folch, A., Costa, A., & Macedonio, G. (2016). FPLUME-1.0: An integral volcanic plume model accounting for ash aggregation. *Geoscientific Model Development*, *9*(1), 431–450. https://doi.org/10.5194/gmd-9-431-2016

Girault, F., Carazzo, G., Tait, S., & Kaminski, E. (2016). Combined effects of total grain-size distribution and crosswind on the rise of eruptive volcanic columns. *Journal of Volcanology and Geothermal Research*, *326*, 103–113. https://doi.org/10.1016/j.jvolgeores.2015.11.007

Hewett, T., Fay, J., & Hoult, D. (1971). Laboratory experiments of smokestack plumes in a stable atmosphere. *Atmospheric Environment*, *5*, 767–789. https://doi.org/10.1016/0004-6981(71)90028-X

Hoult, D., Fay, J., & Forney, L. (1969). A theory of plume rise compared with field observations. *Journal of the Air Pollution Control Association*, *19*, 585–590. https://doi.org/10.1080/00022470.1969.10466526

Jessop, D., Gilchrist, J., Jellinek, A., & Roche, O. (2016). Are eruptions from linear fissures and caldera ring dykes more likely to produce pyroclastic flows? *Earth and Planetary Science Letters*, *454*, 142–153. https://doi.org/10.1016/j.epsl.2016.09.005

Kalnay, E., Kanamitsu, M., Kistler, R., Collins, W., Deaven, D., Gandin, L., … Joseph, D. (1996). The NCEP/NCAR 40-year reanalysis project. *Bulletin of the American Meteorological Society*, *77*(3), 437–471. https://doi.org/10.1175/1520-0477(1996)077

Kaminski, E., Tait, S., & Carazzo, G. (2005). Turbulent entrainment in jets with arbitrary buoyancy. *Journal of Fluid Mechanics*, *526*, 361–376. https://doi.org/10.1017/S0022112004003209

Mastin, L. (2014). Testing the accuracy of a 1-D volcanic plume model in estimating mass eruption rate. *Journal of Geophysical Research: Atmospheres*, *119*, 2474–2495. https://doi.org/10.1002/2013JD020604

Morton, B. R., Taylor, G., & Turner, J. S. (1956). Turbulent gravitational convection from maintained and instantaneous sources. *Proceedings of the Royal Society of London A: Mathematical, Physical and Engineering Sciences*, *234*(1196), 1–23. https://doi.org/10.1098/rspa.1956.0011

Robock, A. (2000). Volcanic eruptions and climate. *Reviews of Geophysics*, *38*, 191–219. https://doi.org/10.1029/1998RG000054

Suzuki, Y., & Koyaguchi, T. (2015). Effects of wind on entrainment in volcanic plumes. *Journal of Geophysical Research: Solid Earth*, *120*, 6122–6140. https://doi.org/10.1002/2015JB012208

Tate, P. M. (2002). The rise and dilution of buoyant jets and their behaviour in an internal wave field (PhD thesis), University of New South Wales, Sidney, Australia.

Woodhouse, M. J., Hogg, A. J., Phillips, J. C., & Rougier, J. C. (2015). Uncertainty analysis of a model of wind-blown volcanic plumes. *Bulletin of Volcanology*, *77*(10), 1–28. https://doi.org/10.1007/s00445-015-0959-2

Woodhouse, M., Hogg, A., Phillips, J., & Sparks, R. S. J. (2013). Interaction between volcanic plumes and wind during the 2010 Eyjafjallajökull eruption, Iceland. *Journal of Geophysical Research: Solid Earth*, *118*, 92–109. https://doi.org/10.1029/2012JB009592